Elastic and inelastic electron-nucleus scattering form factors of some light nuclei: ^{23}Na, ^{25}Mg, ^{27}Al, and ^{41}Ca

Khalid S. Jassim,[1,2,*] Anwer A. Al-Sammarrae,[1,3] Fadhil I. Sharrad,[4] and Hasan Abu Kassim[1]
[1]*Department of Physics, Quantum Science Centre, Faculty of Science, University of Malaya, 50603 Kuala Lumpur, Malaysia*
[2]*Department of Physics, College of Education for Pure Science, University of Babylon, P.O. Box 4, Hilla-Babylon, Iraq*
[3]*Department of Chemistry, College of Education, University of Samarra, Selah Alden, Iraq*
[4]*Department of Computer Science, College of Science, University of Karbala, Karbala, Iraq*
(Received 18 July 2013; revised manuscript received 2 November 2013; published 7 January 2014)

Nuclear structure (energy levels, elastic and inelastic electron-nucleus scattering, and transition probability) of ^{23}Na, ^{25}Mg, ^{27}Al, and ^{41}Ca nuclei have been studied using shell-model calculations. A set of two-body interactions are used in this paper. The universal *sd* of the Wildenthal interaction in the proton-neutron formalism, universal *sd*-shell interaction A, universal *sd*-shell interaction B, and GXFP1 interaction for the *fp* shell is used with the nucleon-nucleon realistic interaction Michigan three-range Yakawa as a two-body interaction for core-polarization calculations. Two shell-model codes, CPM3Y and NUSHELL for Windows, have been used to calculate the results. The wave functions of radial single-particle matrix elements have been calculated with harmonic-oscillator and Woods-Saxon potentials. The level schemes are compared with the experimental data up to 5.776, 5.251, and 4.51 MeV for ^{23}Na, ^{25}Mg, and ^{27}Mg, respectively. Very good agreements are obtained for all nuclei in this study. Results from electron scattering form-factor calculations have shown that the core-polarization effects are essential to obtain a reasonable description of the data with no adjustable parameters.

DOI: 10.1103/PhysRevC.89.014304 PACS number(s): 25.30.Bf, 25.30.Dh, 21.60.Cs, 27.30.+t

I. INTRODUCTION

The two-body effective interaction is a key ingredient for the success of the nuclear shell model, which determines the accuracy of the shell-model calculations that assume an appropriate core to be inert and a limited space (the so-called model space and sufficient computing methods). The effective interaction is used to understand nuclear properties microscopically by starting with the realistic nucleon-nucleon (NN) interaction and using quantum-mechanical many-body theory. The earliest shell-model calculations [1] used a simple square well potential between nucleons, but 50 years of research have led to better interactions. The established shell-model codes require an interaction to be constructed from single-particle energies (SPEs) and two-body matrix elements (TBMEs), given by $\langle ab|V|cd\rangle_{JT}$, where a, b, c, and d are single-particle orbits, V is an effective two-body interaction, and J and T are the spin and isospin of the coupled nucleons. In shell-model calculations, to solve the eigenvalue problem, many shell-model codes have been developed, such as OXBASH [2], ANTOINE [3], NUSHELL [4], and NUSHELLX [5]. The effects of core polarization (CP) on the nuclear form factor were found to be necessary for enhancing the calculations to compare with the experimental data [6,7]. The Michigan three-range Yukawa (M3Y) interaction [8] has been derived from the realistic NN interaction by fitting the Yukawa functions to the G matrix. Represented by the sum of the Yukawa functions, the M3Y-type interactions will be tractable in various models. It has been shown that the M3Y interaction gave matrix elements similar to some reliable shell-model interactions [9]. Moreover, with certain modifications, M3Y-type interactions have successfully been applied to nuclear reactions [10], including electron scattering. A class of the M3Y-type interactions can be applied to the electron scattering form-factor calculations by utilizing Elliott fitting. In this paper, we will use the M3Y-Elliott-type interaction as a residual interaction and will investigate the modification in the calculations. The universal *sd* of the Wildenthal interaction (USD) Hamiltonian [11] has provided realistic *sd*-shell ($0d_{5/2}$,$0d_{3/2}$,$1s_{1/2}$) wave functions for use in nuclear structure models, nuclear spectroscopy, and nuclear astrophysics for over two decades. It is also an important part of the Hamiltonian used for the *p*-*sd* [12] and *sd*-*pf* [13–15] model spaces [16]. The USD Hamiltonian is based on 63 TBMEs and three SPEs given in Table I of Ref. [8]. The universal *sd*-shell interaction B (USDB) and the universal *sd*-shell interaction A (USDA) in the proton-neutron formalism are a new USD-type Hamiltonian based on 66 parameters to fit 608 energy data in *sd*-shell nuclei ($A = 16$–40) with a root-mean-square deviation of 130 and 170 keV, respectively [16,17]. These new interactions have clearly resolved the fluorine problem as well as all of the oxygen isotopes [16]. The single-particle energies for the $0d_{3/2}$, $0d_{5/2}$, and $1s_{1/2}$ orbitals are (in MeV) -1.9798, -3.9436, and -3.0612 for the USDA interaction and -2.1117, -3.9257, and -3.2079 for the USDB interaction.

Recently, electron scattering form factors with transition probabilities have been calculated [18] for different states in ^{10}B, ^{32}Sc, and ^{48}Ca nuclei by using nuclear shell-model calculations. The results with the inclusion of CP effects modify the form factors markedly and describe the experimental values very well in the range of the momentum transfer (q) values. Transverse electron scattering form factors of the first three levels of the ^{25}Mg nucleus have been calculated [19] by using the Nilsson model of deformed nuclei with and without collective contributions. The results for the energy

*Khalid_ik74@yahoo.com

levels considered give good overall agreement, although there is no clear distinction between the various approximations for the rotational current in the experimental data.

The present study is divided into two parts; the first part is to calculate the energy levels and the probability current density with different two-body effective interactions as a residual interaction by using the shell-model code NUSHELL for Windows. The USD-type Hamiltonians USDA and USDB and the USD [20] interaction have been used to give the ($0d_{5/2}$, $1s_{1/2}$, and $0d_{3/2}$) shell-model wave function for ^{23}Na, ^{25}Mg, and ^{27}Al. GXPF1 [21] has been used to give the ($0f_{7/2}$, $0f_{5/2}$, $1p_{3/2}$, and $1p_{1/2}$) shell-model wave functions for ^{41}Ca. The second part is to calculate the longitudinal and transverse electron scattering form factors from sd- and fp-shell nuclei (^{23}Na, ^{25}Mg, ^{27}Al, and ^{41}Ca) by using the shell-model codes CPM3Y (with and without inclusion core-polarization effects) and NUSHELL. The modern M3Y nucleon-nucleon interaction is used for CP effect calculations [8]. The single-particle matrix elements have been calculated with harmonic-oscillator (HO) and Woods-Saxon (WS) potentials.

The aim of the present paper is to consider the particle-hole excitation of the core and the model space to calculate the electron scattering form factor. We adopt the USD and USDA wave functions for the zero-order wave functions and examine the effects of the core polarization with the M3Y interaction. Within this model, we do not introduce any state-dependent effective charges, effective g factors, or any adjustable parameters. Also, we make a comparison between the experimental data and the theoretical calculation for the energy levels and $B(E2)$ by using the above three effective interactions.

II. THEORY

The reduced matrix elements of the electron scattering operator $\hat{T}^{\eta}_{\Lambda}$ consist of two parts, one is for the model-space (MS) matrix elements, and one is for the CP matrix elements [22],

$$\langle \mathrm{X}_f \| \hat{T}^{\eta}_{\Lambda} \| \mathrm{X}_i \rangle = \langle \mathrm{X}_f \| \hat{T}^{\eta}_{\Lambda} \| \mathrm{X}_i \rangle_{\mathrm{MS}} + \langle \mathrm{X}_f \| \delta\hat{T}^{\eta}_{\Lambda} \| \mathrm{X}_i \rangle_{\mathrm{CP}}, \tag{1}$$

where states $|\mathrm{X}_i\rangle$ and $|\mathrm{X}_f\rangle$ are described by the model-space wave functions. Greek symbols are used to denote quantum numbers in coordinate space and isospin, i.e., $\mathrm{X}_i \equiv J_i T_i$, $\mathrm{X}_f \equiv J_f T_f$, and $\Lambda \equiv JT$.

The MS matrix elements are expressed as the sum of the product of the one-body density-matrix elements (OBDMs) times the single-particle matrix elements, which is given by

$$\langle \mathrm{X}_f \| \hat{T}^{\eta}_{\Lambda} \| \mathrm{X}_i \rangle_{\mathrm{MS}} = \sum_{\alpha,\beta} O^{\mathrm{X}}_{\mathrm{X}_i \mathrm{X}_f}(\alpha,\beta) \langle \alpha \| \hat{T}^{\eta}_{\Lambda} \| \beta \rangle_{\mathrm{MS}}, \tag{2}$$

where α and β denote the final and initial single-particle states, respectively (isospin is included) for the model space. $O^{\mathrm{X}}_{\mathrm{X}_i \mathrm{X}_f}$ are the OBDM elements.

Similarly, the CP matrix element can be written as

$$\langle \mathrm{X}_f \| \delta\hat{T}^{\eta}_{\Lambda} \| \mathrm{X}_i \rangle_{\mathrm{CP}} = \sum_{\alpha,\beta} O^{\mathrm{X}}_{\mathrm{X}_i \mathrm{X}_f}(\alpha,\beta) \langle \alpha \| \delta\hat{T}^{\eta}_{\Lambda} \| \beta \rangle_{\mathrm{CP}}. \tag{3}$$

By using the first-order perturbation theory, the single-particle matrix element for the higher-energy configurations outside the core and MS is given by [23]

$$\langle \alpha | \delta\hat{T}^{\eta}_{\Lambda} | \beta \rangle = \langle \alpha | V_{12} \frac{\mathrm{P}}{E_i - H^{(0)}} \hat{T}^{\eta}_{\Lambda} | \beta \rangle + \langle \alpha | \hat{T}^{\eta}_{\Lambda} \frac{\mathrm{P}}{E_f - H^{(0)}} V_{12} | \beta \rangle, \tag{4}$$

where P is the projection operator onto the space outside the model space and V_{12}'s are adopted as a residual two-body interaction. E_i and E_f are the energies of the initial and final states, respectively. $H^{(0)}$ is the unperturbed Hamiltonian. Equation (4) is written as [23]

$$\begin{aligned} &\langle \alpha \| \delta\hat{T}_{\Lambda} \| \beta \rangle \\ &= \sum_{\alpha_1,\alpha_2,\Gamma} \frac{(-1)^{\beta+\alpha_2+\Gamma}}{e_\beta - e_\alpha - e_{\alpha_1} + e_{\alpha_2}} (2\Gamma+1) \begin{Bmatrix} \alpha & \beta & \Lambda \\ \alpha_2 & \alpha_1 & \Gamma \end{Bmatrix} \\ &\quad \times \langle \alpha\alpha_1 | V_{12} | \beta\alpha_2 \rangle_{\mathrm{X}} \langle \alpha_2 \| \hat{T}^{\eta}_{\Lambda} \| \alpha_1 \rangle \\ &\quad \times \sqrt{(1+\delta_{\alpha_1\alpha})(1+\delta_{\alpha_2\beta})} + \mathrm{A}, \end{aligned} \tag{5}$$

where A represents additional terms with α_1 and α_2 exchanged with an overall minus sign. The indices α_1 and α_2 run over particle and hole states, respectively, and e is the single-particle energy. The CP parts allow particle-hole excitations from the core and model space into higher orbits. These excitations are taken up to $4\hbar\omega$.

The reduced single-particle matrix element becomes

$$\langle \alpha_2 \| \hat{T}^{\eta}_{JT} \| \beta_1 \rangle = \sqrt{\frac{2T+1}{2}} \sum_{t_z} I_T(t_z) \langle \alpha_2 \| \hat{T}^{\eta}_{Jt_z} \| \alpha_1 \rangle, \tag{6}$$

where

$$I_T(t_z) = \begin{cases} 1 & \text{for} \quad T = 0, \\ (-1)^{1/2-t_z} & \text{for} \quad T = 1, \end{cases} \tag{7}$$

and $t_z = 1/2$ and $-1/2$ for the proton and neutron, respectively.

Elastic and inelastic electron scattering form factors in terms of angular momentum J and momentum transfer q, between the initial and final states of spin $J_{i,f}$ and isospin $T_{i,f}$, are given by [24]

$$\left|F^{\eta}_{J}(q)\right|^2 = \frac{4\pi}{Z^2(2J_i+1)} \left| \sum_{T=0,1} (-1)^{T_f - T_{zf}} \begin{pmatrix} T_f & T & T_i \\ -T_{Zf} & M_T & T_{Zi} \end{pmatrix} \langle \mathrm{X}_f \| T^{\eta}_{J,T}(q) \| \mathrm{X}_i \rangle \right|^2 |F_{\mathrm{cm}}(q)|^2 \times |F_{\mathrm{fs}}(q)|^2, \tag{8}$$

where T_z is the projection along the z axis of the initial and final isospin states. $F_{\mathrm{fs}}(q) = \exp(-0.43q^2/4)$ is the nucleon finite-size (fs) form factor and $F_{\mathrm{cm}}(q) = \exp(q^2b^2/4A)$ is the correction for the lack of translation invariance in the shell model. A and b are the mass number and the harmonic-oscillator size parameter, respectively.

The single-particle energies are given by [23]

$$e_{nlj} = \left(2n + l - \tfrac{1}{2}\right)\hbar\omega + \begin{cases} -\frac{1}{2}(l+1)\langle f(r)\rangle_{nl} & \text{for} \quad j = l - \frac{1}{2}, \\ \frac{1}{2}l\langle f(r)\rangle_{nl} & \text{for} \quad j = l + \frac{1}{2}, \end{cases} \tag{9}$$

with

$$\langle f(r)\rangle_{nl} \approx 20A^{-2/3}\text{MeV}, \qquad \hbar\omega = 45A^{-1/3} - 25A^{-2/3}. \tag{10}$$

The realistic M3Y effective NN interaction, which is used in the electron scattering v_{12}, is expressed as a sum of the central potential part v_{12}^{C}, spin-orbit potential part v_{12}^{LS}, and long-range tensor part V_{12}^{TN} as follows [25]:

$$V_{12} = V_{12}^{(c)} + V_{12}^{(LS)} + V_{12}^{(TN)}. \tag{11}$$

The two-body matrix elements of the realistic M3Y effective NN interaction consist of three parts: the central matrix element, the spin-orbit matrix element, and the tensor matrix element,

$$\langle j_1 j_2|V_{12}|j_3 j_4\rangle_\Gamma = \langle j_1 j_2|V_{12}^{c}|j_3 j_4\rangle_\Gamma + \langle j_1 j_2|V_{12}^{LS}|j_3 j_4\rangle_\Gamma + \langle j_1 j_2|V_{12}^{TN}|j_3 j_4\rangle_\Gamma. \tag{12}$$

The reduced transition probability is related to the form factor at the photon point, which is given by [26]

$$B(CJ) = \frac{|(2J+1)!!|^2}{4\pi}\frac{Z^2e^2}{k^{2L}}\left|F_J^{\text{Co}}(q=k)\right|^2, \tag{13}$$

where $q = k = \frac{E_x}{\hbar c}$ is the momentum transfer and the term $|F_J^{\text{Co}}(q=k)|^2$ is the longitudinal (Coulomb) form factor at $k = q$, which is given by

$$\left|F_J^{\text{Co}}(k)\right|^2 = \frac{4\pi}{(2J_i+1)}\frac{1}{Z^2}\left|\int_0^\infty dr\, r^2 j_J(kr)\rho_J(i,f,r)\right|^2. \tag{14}$$

Here $\rho_J(i,f,r)$ is the transition charge density for the initial and final states.

For the two-body matrix elements of the residual interaction $\langle\alpha\alpha_2|V_{12}|\beta\alpha_1\rangle_\Gamma$, which appear in Eqs. (5) and (11), the M3Y interaction of Bertch *et al.* [8] is adopted. The interaction is taken between a nucleon in any core orbit and a nucleon that is excited to higher orbits with the same parity and with the required multipolarity (Λ) and between a nucleon in any *sd* orbits and that is excited to higher orbits with the same parity and with the required multipolarity. This interaction is given in the *LS* coupling.

III. RESULTS AND DISCUSSION

A. Energy levels and probability current density

The energy levels and probability current density calculations have been performed in the *sd* model space with the shell-model code NUSHELL since we are interested in the positive-parity states of ^{23}Na, ^{25}Mg, and ^{27}Al for the valance neutrons and protons states ($0d_{5/2}$,$0d_{3/2}$,$1s_{1/2}$) outside the core ^{16}O for shell nuclei. Theoretical energy levels for the ^{23}Na nucleus are plotted in the second (USDA), third (USDB), and fourth (USD) columns in Fig. 1 and are compared with the experimental spectrum [27] in the first column. The agreement is excellent for $J^\pi = 3/2_1{}^+$ and $5/2_1{}^+$ states when compared with the experimental data. The energy differences between the $7/2_1$ and the $1/2_1{}^+$ states are 0.048 and 0.004 MeV with USDA and USDB effective interactions, respectively, whereas, the experimental energy difference is 0.31 MeV. The second $3/2^+$ is predicted at 2.771 MeV by USDA, 2.723 MeV by USDB, and 2.743 MeV by USD interactions, whereas, the corresponding experimental value is 2.98 MeV. The $5/2_2{}^+$, $1/2_2{}^+$, and $7/2_2{}^+$ excited states are predicted at about 3.887, 4.307, and 4.632 MeV, respectively. In our calculation, a $5/2_3{}^+$ level is predicted at 5.513, 5.423, and 5.242 MeV for USDA, USDB, and USD, respectively. The $11/2_1{}^+$ also is very well predicted by USDA and USDB interactions. The calculated $9/2_1{}^+$ state is at 6.098, 6.023, and 5.945 MeV for USDA, USDB, and USD interactions, respectively, compared to the experimental value (Ref. [27]) of 6.114 MeV.

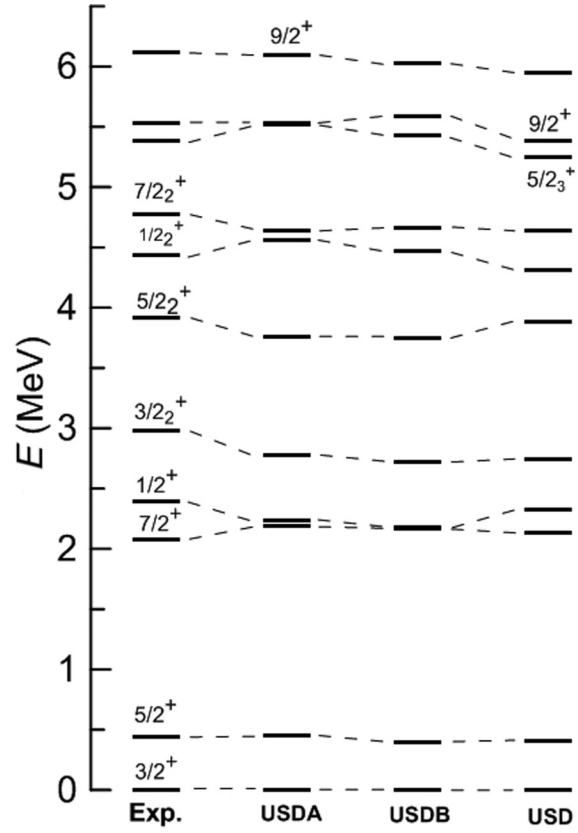

FIG. 1. Energy levels of the ^{23}Na nucleus from the experimental data in Ref. [27] are compared to the shell-model results with three effective interactions USD, USDA, and USDB.

The energy levels of the three lowest states in the ^{25}Mg scheme are calculated with the NUSHELL code and are compared with the experimental data [28]. We are interested in five neutrons and four protons in the model space ($0d_{5/2}$,$1s_{1/2}$,$0d_{3/2}$) outside the ^{16}O core. Figure 2 shows the calculated energy levels by the three different interactions

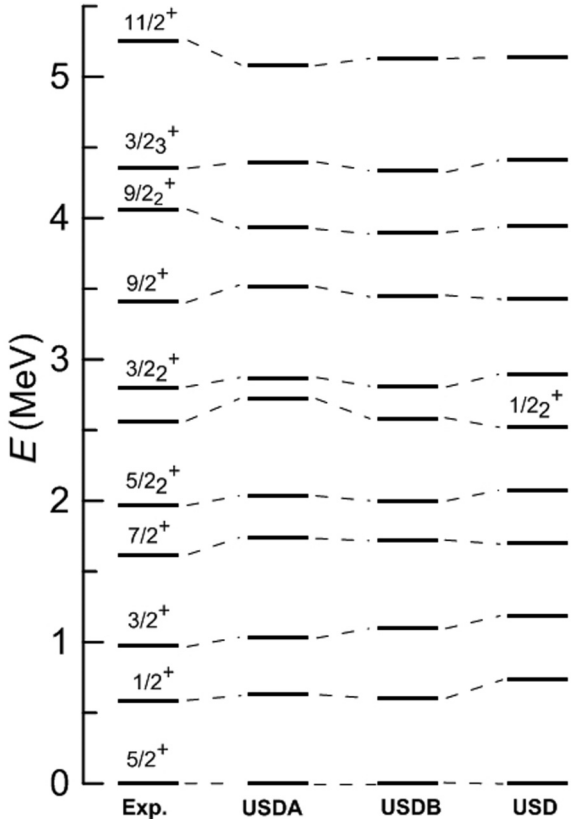

FIG. 2. Energy levels of the ^{25}Mg nucleus from the experimental data in Ref. [28] are compared to the shell-model results with three effective interactions USD, USDA, and USDB.

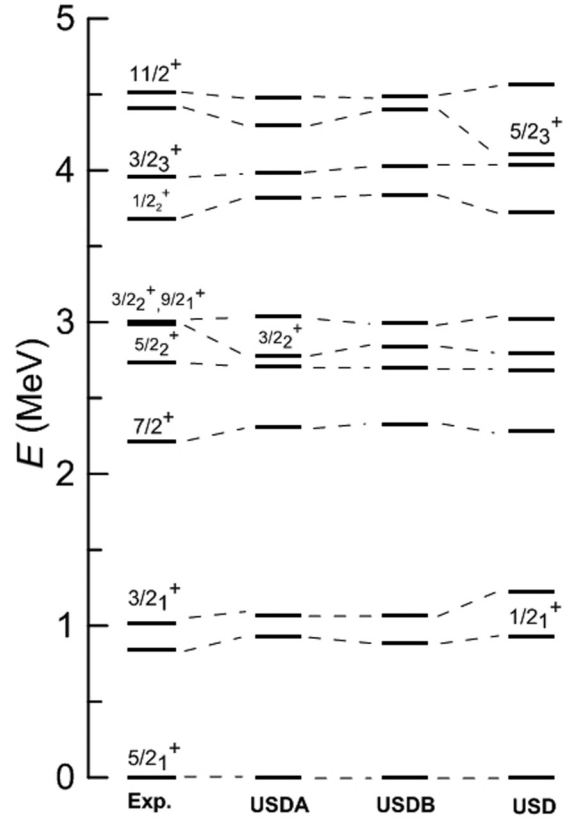

FIG. 3. Energy levels of the ^{27}Al nucleus from the experimental data in Ref. [30] are compared to the shell-model results with three effective interactions USD, USDA, and USDB.

compared with the experimental data. The $5/2^+$ ground state is reproduced correctly by all of the interactions. The energy levels are well predicated for states $1/2_1{}^+$ and $3/2_1{}^+$ by USDA and USDB, whereas, the USD interaction predicts 0.734 and 1.186 MeV for the $1/2_1{}^+$ and $3/2_1{}^+$ states, respectively, higher than the experimental values of 0.585 and 0.974 MeV. Good agreement is obtained between the calculated results and experimental data for states $7/2^+$, $5/2_3{}^+$, and $3/2_3{}^+$, respectively. The calculated $1/2_2{}^+$ state is at 2.723 MeV for USDA, 2.583 MeV for USDB, and 2.519 MeV for USD interactions compared to the experimental value of 2.563 MeV.

Nuclear structure studies on the ^{27}Al nucleus are interesting because this nucleus lies in a transitional region of mass number where the nuclear deformation changes from prolate (for ^{26}Mg) to oblate (for ^{28}Si) [29]. In Fig. 3, we have shown the comparison of the experimental values with those predicted for the three different interactions. The $5/2^+$ ground state is reproduced correctly by the USDA, USDB, and USD interactions. The $3/2_1{}^+$ state is very well predicted by the USDA and USDB interactions, whereas, the USD interaction predicts a higher energy than the experimental value. The calculated energy levels of states $5/2_2{}^+$, $9/2_1{}^+$, and $3/2_3{}^+$ for all the three effective interactions are in very good agreement with the experimental data. The USD interaction gives very good agreement for state $1/2_2{}^+$, whereas, the USDA and USDB interactions predict the 3.833- and 3.724-MeV energies, respectively, higher than the experimental data. The energy of the $5/2_3{}^+$ state deviates from the experimental value by 9% and 13% for USDA and USDB interactions, respectively, whereas, the USD interaction deviates by 35%. The agreement is excellent for states $11/2_1{}^+$ for both the USDA and the USDB interactions, whereas, the USD interaction predicts it 0.051 MeV higher than the experimental value.

The calculated transition probability $B(E2)$ results for different states of some sd-shell nuclei are compared with the experimental data, which are given in Table I . The $B(E2)$ values for $(1/2_1{}^+ \rightarrow 5/2_1{}^+)$ and $(3/2_1{}^+ \rightarrow 5/2_1{}^+)$ transitions of the ^{25}Mg nucleus give much closer to the experimental values for all effective interactions. In our calculations, the $B(E2)\downarrow$ $(7/2_1{}^+ \rightarrow 5/2_1{}^+)$ transition probabilities for the ^{23}Na nucleus are predicted at 62.1, 67.470, and 22.44 e^2 fm^4 for the USDB, USD, and USDA interactions respectively, whereas, the experimental value is at 64.489 e^2 fm^4. The $B(E2)$ transition probabilities for the $(1/2_1{}^+ \rightarrow 5/2_1{}^+)$ and $(3/2_1{}^+ \rightarrow 5/2_1{}^+)$ transitions of ^{27}Al with the USD interaction give good agreement with the experimental value.

B. Electron Scattering Form Factor

A computer program, CPM3Y in FORTRAN 90 was written to calculate the model-space form factors (zeroth-order) and the first-order CP effects of the M3Y interaction. The OBDM elements are calculated by using the shell-model NUSHELL code with USD and USDA effective interactions.

TABLE I. Experimental [27,28,30] and theoretical reduced transition probabilities, $B(E2)\downarrow$ for the positive-parity states in ^{23}Na, ^{25}Mg, and ^{27}Al nuclei calculated with the effective charges $e_p = e_n = 0.35e$ for protons and neutrons. The theoretical $B(E2)\downarrow$ values have been calculated by using the NUSHELL code.

Nuclei	$J_i \rightarrow J_f$	$B(E2)$ (e^2 fm^4)			
		Expt.	USDA	USDB	USD
^{23}Na	$7/2_1^+ \rightarrow 3/2_1^+$	49.338 (11)	41.47	40.440	42.520
	$7/2_1^+ \rightarrow 5/2_1^+$	64.489 (22)	56.69	62.100	67.470
^{25}Mg	$1/2_1^+ \rightarrow 5/2_1^+$	2.444 (10)	3.704	2.964	2.425
	$3/2_1^+ \rightarrow 1/2_1^+$	47.758 (5)	35.690	67.770	67.500
	$3/2_1^+ \rightarrow 5/2_1^+$	3.95 (13)	4.795	4.103	4.255
^{27}Al	$1/2_1^+ \rightarrow 5/2_1^+$	37.524 (23)	49.450	50.320	46.470
	$3/2_1^+ \rightarrow 5/2_1^+$	37.524 (7)	52.630	51.320	50.450
	$5/2_2^+ \rightarrow 3/2_1^+$	41.854 (18)	35.090	34.210	33.600

Elastic longitudinal $C0 + C2$ form factors for the $3/2^+$ (0.0-MeV) state of the ^{23}Na nucleus calculated with CP effects on the sd-shell model wave function are shown in Fig. 4. The CP effects with the M3Y realistic interaction are included by allowing particle-hole excitation from $(0s_{1/2},0p_{1/2},0p_{3/2},0d_{5/2},1s_{1/2},0d_{3/2})$ shells up to higher shells with $6\hbar\omega$ excitations. The USDA interaction has been used to calculate the multipole decompositions $C0$ and $C2$. The total form factor with CP effects is shown by the solid curve where the data are in very good agreement for the whole momentum-transfer range (0–2.5 fm^{-1}). All calculations were performed using the HO wave function with size parameter $b = 1.80$ fm [31]. The experimental data are taken from Ref. [32]. The contributions of $M1$ and $M3$ form factors and their sum are shown in Fig. 5 where the solid curve represents the calculation

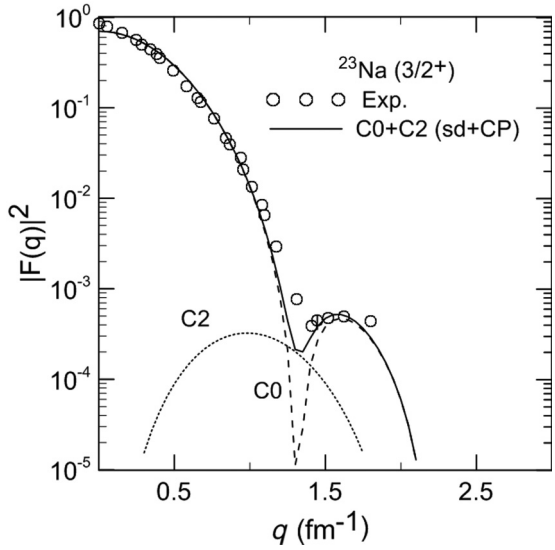

FIG. 4. Elastic longitudinal $C0 + C2$ form factors for the $3/2^+$ (0.0-MeV) state in the ^{23}Na nucleus, calculated with core-polarization effects on the sd-shell-model wave function. The experimental data are taken from Ref. [32].

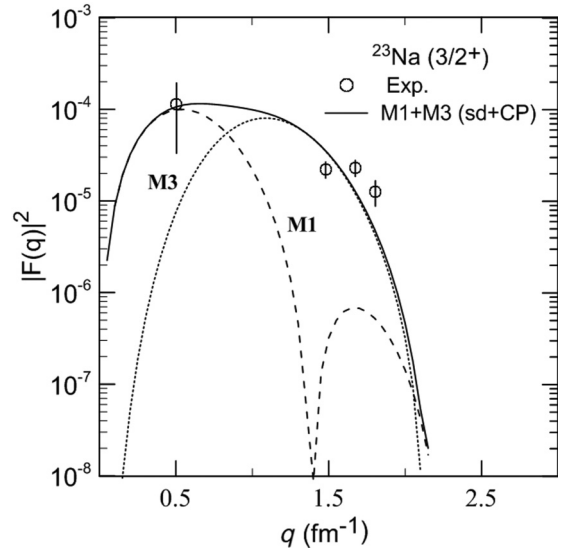

FIG. 5. Elastic transverse $M1 + M3$ form factors for the $3/2^+$ (0.0-MeV) state in the ^{23}Na nucleus, calculated with core-polarization effects on the sd-shell-model wave function. The experimental data are taken from Ref. [32].

of the sd-shell model space with core-polarization effects by using the USDA effective interaction for the model space and the M3Y realistic interaction as a residual interaction for the CP effect calculation, the dashed curve represents the calculation of the transverse $M1$, and the dotted curve represents the transverse $M3$. A congruency in the form factors is noticed in comparison with the experimental data, although only a few experimental values are available.

The electron excites the ^{25}Mg nucleus from the ground state to the $7/2_1^+$ state with an excitation energy of 1.698 MeV. The transverse form factor for this transition has mixed multipolarities $M1 + E2 + M3 + M5$. The total transverse form-factor isovector transition is shown in Fig. 6. The individual multipoles also are shown. The main contribution in most of the regions of q comes from $M1$ and $M5$. $M1$ has the dominant contribution in the region between 0 and 1.2 fm^{-1}, and $M5$ has the dominant contribution in the range of momentum transfer from 0.5 to 3.0 fm^{-1}. The results of the total transverse form factor (as a solid curve) give good agreement, compared with the available experimental data [19].

Figure 7 shows the calculation of the total contribution of $E2$, $M3$, and $M5$ multipoles for the USDA effective interaction for the $9/2^+$ (3.515 MeV) state in the ^{25}Mg nucleus by using the HO wave function. The individual multipoles also are shown in the same figure. One can see that the $M5$ (as a dashed curve) is more sensitive to the experimental data [19] and describes it very well in the momentum-transfer range from 1 to 3 fm^{-1}.

Figure 8 shows the calculated inelastic form factors with the inclusion of the CP effect by using the CPM3Y (as the solid curve) and the NUSHELL codes with HO (as the dashed red curve) and WS potential (as the dotted line curve) with three effective interactions (USDA, USDB, and USD) of the

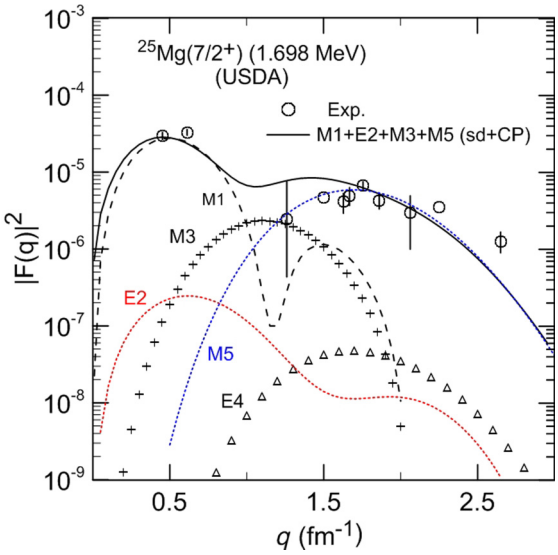

FIG. 6. (Color online) Inelastic transverse form factors for the transition to the $7/2^+$ (1.698-MeV) state in the ^{25}Mg nucleus, calculated with core-polarization effects on the *sd*-shell-model wave function. The experimental data are taken from Ref. [19].

^{27}Al nucleus. It is seen that the effect of these interactions does not significantly affect the calculation of the Coulomb $C2$ form factors as shown in Figs. 8(a)–8(c). The form-factor calculation with the WS potential enhances the form factor and describes the experimental data [33] very well for the minimum diffraction for scattered electrons at the higher momentum-transfer range from 2 to 3 fm^{-1}. The form factors with the inclusion of the CP effect that use CPM3Y are in agreement with the experimental momentum transfer up to 1.7 fm^{-1} but overestimate the data for the momentum transfer

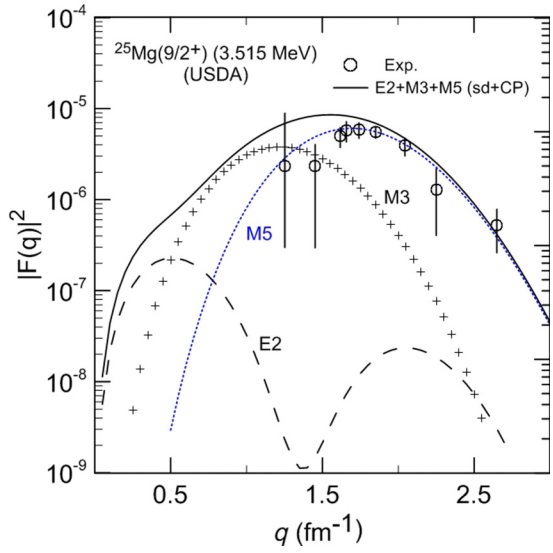

FIG. 7. (Color online) The transverse form factors for the transition to the $9/2^+$ (3.515-MeV) state in the ^{25}Mg nucleus, calculated with core-polarization effects on the *sd*-shell-model wave function. The experimental data are taken from Ref. [19].

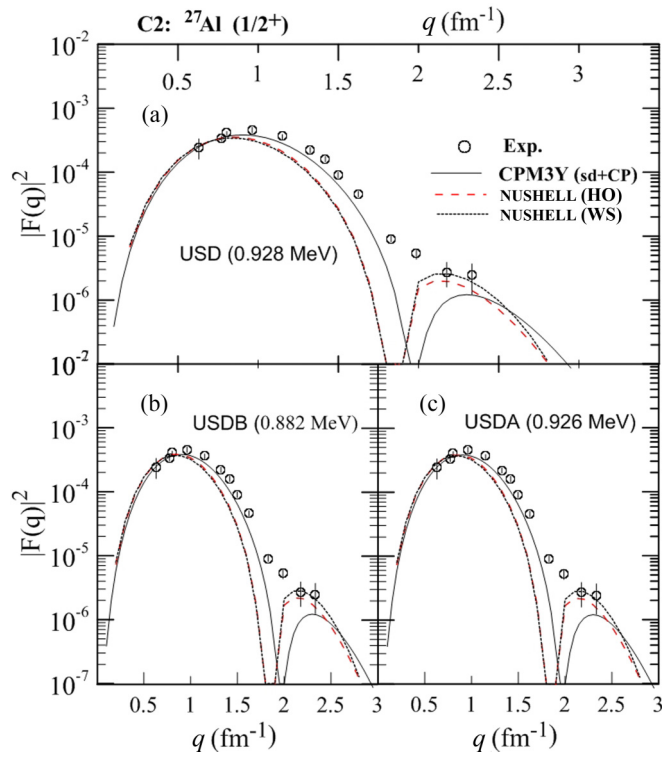

FIG. 8. (Color online) The longitudinal $C2$ form factors for the transition to the $1/2^+$ state in the ^{27}Al nucleus. The upper panel (a) represents the calculated form factors with the USD effective interaction for the *sd* shell, whereas, the lower panels (b) and (c) represent those of the USDA and USDB effective interactions, respectively. The experimental data are taken from Ref. [33].

higher than $q = 1.7$ fm^{-1}. The form-factor calculations that use NUSHELL take into account the collective modes of the nuclei; the CP effects are evaluated by adopting the purely empirical Tassie model [34] together with the calculated ground-state charge-density distribution obtained for the low mass (1*s*-0*d*)-shell nuclei by using the occupation number of the states where subshell 1*s* is included with the occupation number of the protons. The Tassie results shifted the position of the diffraction maximum to lower values. This means that the microscopic CP evaluation with M3Y gives a better agreement with the experimental data than the Tassie model.

The longitudinal form factors for the $3/2^+$ (1.069-MeV) state and $7/2+$ (2.304-MeV) states of the ^{27}Al nucleus are shown in Fig. 9. The maximum diffraction is at $q = 0.9$ and 1 fm^{-1} and for the $3/2^+$ and $7/2^+$ states, respectively. The minimum diffraction for scattered electrons occur at the momentum-transfer values $q = 2.1$ and 2.2 fm^{-1} for the $3/2^+$ and $7/2^+$ states, respectively. The form factors with the NUSHELL code overestimate the experimental data in the first maximum up to $q = 1.6$ fm^{-1}. Beyond that, the calculation with the WS potential gives a better agreement compared to the calculation with the HO potential that uses the CPM3Y code. The $(sd + \mathrm{CP})$ calculations are in slightly better agreement with the experimental data. CP effects enhance the form factor and reproduce the measured form factor in the maximum region of $(0.5 < q < 1.6)$ fm^{-1}, but the calculation with only

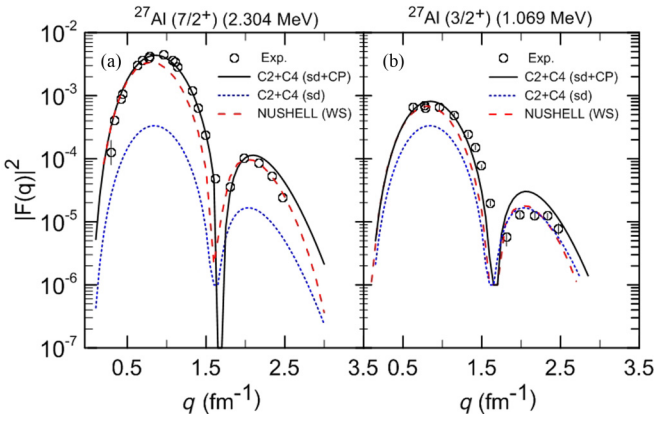

FIG. 9. (Color online) The longitudinal form factors for the transition to the $3/2^+$ at 1.069-MeV [panel (a)] and $7/2+$ at 2.304-MeV [panel (b)] states in the ^{27}Al nucleus, calculated with core-polarization effects on the sd-shell-model wave function by using the USDA effective interaction. The experimental data are taken from Ref. [29]. The solid curves and dotted curves represent the calculation with and without inclusion, respectively, of the CP effect by using the CPM3Y code. The dashed curves represent the calculation that uses the NUSHELL code with the WS potential.

the sd model space, without any inclusion of the CP effects in the $3/2^+$ state, gives good agreement with the experimental data for the second minimum region of $(1.6 < q < 2.7)$ fm^{-1}. In this isoscalar transition, the CP effect leads to an increase in the $C2$ longitudinal form-factor component by about a factor of 2 over the $1p$-shell calculation.

Figure 10 shows that the Coulomb multipoles which contribute to the scattering are $C0$, $C2$, and $C4$ of ^{27}Al for state

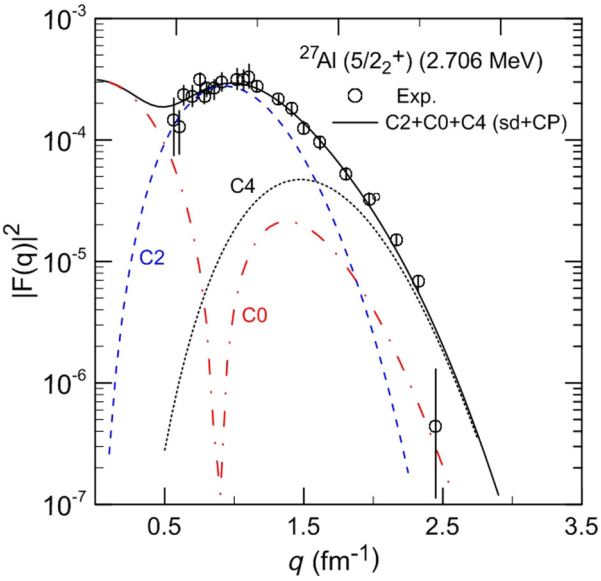

FIG. 10. (Color online) The longitudinal $(C0 + C2 + C4)$ form factors for the transition to the $5/2_2^+$ (2.706-MeV) state in the ^{27}Al nucleus, calculated with core-polarization effects on the sd-shell-model wave function by using the USDA effective interaction. The experimental data are taken from Ref. [29].

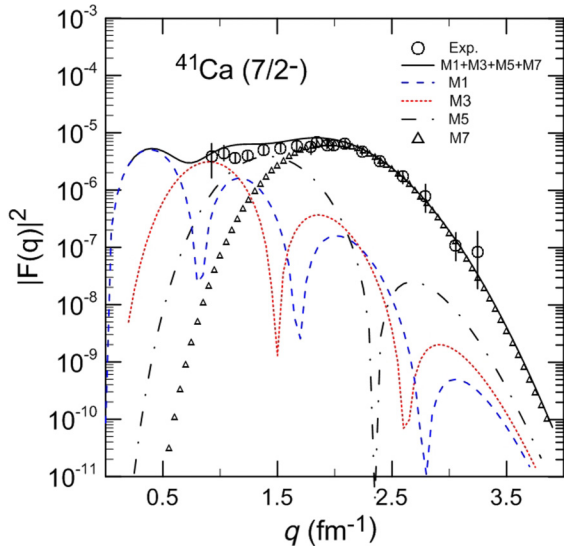

FIG. 11. (Color online) The total transverse form factors for the transition to the $7/2^-$ (MeV) state in the ^{41}Ca nucleus, calculated with core-polarization effects on the sd-shell-model wave function by using the GXPF1 effective interaction. The experimental data are taken from Ref. [36].

$5/2_2^+$ with an excitation energy of 2.706 MeV. The USDA effective interaction for the sd model space with HO wave functions is chosen for the calculation of the Coulomb multipoles in the CPM3Y code. The total form factor $(C0 + C2 + C4)$ with the inclusion of the CP effects gives remarkably good agreement with the experimental data in all regions of the momentum transfer q. The use of the USDA effective interaction for the sd model space that uses the realistic M3Y as a residual interaction of the CP effect enhances the total longitudinal form factor compared with other studies [35].

The total magnetic form factor that represents the total contribution of $M1$, $M3$, $M5$, and $M7$ for the ^{41}Ca $(7/2^-)$ state is shown in Fig. 11. The GXFP1PN effective interaction has been used in the fp-shell-model wave function. It is clear that the total form factor is in very good agreement with the experimental data [36] in the momentum-transfer range from 0.6 to 3.5 fm^{-1}. The $M7$ multipole can be seen to be dominant in the momentum-transfer region covered by the Baghaei *et al.* data [36], especially in the 1.5–3.5-fm^{-1} region. Baghaei *et al.* [36] rightly remarked that the $M5$ component could contribute, but our result shows that $M1$ and $M3$ contribute significantly as well. $M1$ is dominant in the low-momentum region, less than 0.5 fm^{-1} in which experimental data are not available to make a comparison. The distribution of the individual total form factors of different multipolarities indicates that, for the distribution of the form factors with respect to the momentum transfer, there is shifting and quenching in the increase in the q values with the increase in the J values. The experimental data are taken from Ref. [36]. In Figs. 5 and 11, the $E2$ contribution is very small compared with the other multipoles, and for this reason, its effect is not observable in the figures.

IV. CONCLUSION

The nuclear structure (energy levels, reduced transition probabilities, and form factors with and without CP effects) has been calculated for different states in some sd- and fp-shell nuclei by using new effective interactions as a residual interaction, namely, the USDA, USDB, and USD interactions for the ^{23}Na, ^{25}Mg, and ^{27}Al nuclei in the proton-neutron formalism and GXFP1PN for the ^{41}Ca nucleus. These three residual interactions have been used to calculate the sd-model space wave function and have improved, in general, the calculated quantities towards better agreement with the available data for energy levels and form factors at lower values of q, especially for the ^{23}Na and ^{25}Mg nuclei. The energy-level calculation for the $3/2_1{}^+$ and $5/2_1{}^+$ states gives good agreement for ^{23}Mg for the three effective interactions. The USD interaction produces good agreement for states $7/2_1{}^+$, $1/2_1{}^+$, $5/2_2{}^+$, $1/2_2{}^+$, and $7/2_2{}^+$ when compared with the experimental data, whereas, the USDB and USDA interactions make predictions for the two states $5/2_3{}^+$ and $11/2_1{}^+$, respectively. For ^{25}Mg nuclei, all the effective interactions agree with the experimental data, whereas, these effective interactions give the best prediction for states $5/2_1{}^+$, $1/2_1{}^+$, $3/2_1{}^+$, $7/2_1{}^+$, $5/2_2{}^+$, $3/2_2{}^+$, and $11/2_1{}^+$ for the ^{27}Al nucleus.

The use of a modern interaction, such as USDA, USDB, and USD, for model-space calculations and the realistic interaction M3Y in CP effect calculations may give a better description of the form factors. The effect of core polarization is found to be essential for both the transition strengths and the momentum-transfer dependence and gives a good description of the data without any adjustable parameters. The Coulomb ($C2$) form factors at high-q values are successfully described in the ^{27}Al nucleus where the radial part of the single-particle wave function is of the WS potential, rather than the HO potential. Elastic longitudinal ($C0+C2$) form factors for the $3/2^+$ (0.0-MeV) state in the ^{23}Na nucleus, calculated with core polarization on the sd-shell-model wave function, by incorporating the USDA, give a good description. The longitudinal form factor for the $3/2^+$ (1.069-MeV) and $7/2+$ (2.304-MeV) states of the ^{27}Al nucleus that use the NUSHELL code overestimates the experimental results of the first maximum up to $q=1.6$ fm^{-1}; the calculations with the WS potential give a good agreement at high-q data compared to the results with the HO potential that use the CPM3Y code. CP effects enhance the form factor and reproduce the experimental data for all momentum transfers. For the $9/2^+$ (3.515-MeV) state of ^{25}Mg, we can conclude that $M5$ is more sensitive to the experimental data, and it describes it very well in the momentum-transfer range from 1 to 3 fm^{-1}. The total magnetic form factors ($M1$, $M3$, $M5$, and $M7$) for the ^{41}Ca ($7/2^-$) state that uses the GXFP1PN effective interaction agree well with the experimental data in the momentum-transfer range from 0.6 to 3.5 fm^{-1}. The $M7$ multipole is, thus, dominant in the momentum-transfer region between 0.5 and 3.5 fm^{-1} where a large contribution from the $M5$ component could also be expected. The $M1$ form factor is dominant in the low-momentum region less than 0.5 fm^{-1}, which does not have any experimental data in this area.

ACKNOWLEDGMENTS

We thank Professor R. A. Radhi (Department of Physics, College of Science, Department of Physics, University of Baghdad) for providing us with the CPM3Y code. We thank the University of Malaya, the University of Karbala, the University of Babylon, and the University of Samarra for supporting this work. F. Sharrad would like to thank the Islamic Development Bank for support with a postdoctoral fellowship at the University of Malaya in 2011–2012. K. S. Jassim expresses his gratitude to the University of Malaya for support with the Visiting Research Fellow appointment in 2012–2013. A. A. Al-Sammarrae and H. A. Kassim acknowledge support for this work through the University of Malaya Postgraduate Research Grant No. PV089/2011A. We acknowledge the help of M. Bennett for proofreading this paper and for giving some constructive comments.

[1] K. A. Brueckner, Phys. Rev. **96**, 508 (1954).
[2] B. A. Brown, A. Etchegoyen, W. D. M. Rae, N. S. Godwin, W. A. Richter, C. H. Zimmerman, W. E. Ormand, and J. S. Winfield, MSU-NSCL Report No. 524, 1985.
[3] E. C. A. F. Nowacki, Acta Phys. Pol. B **30**, 705 (1999).
[4] B. A. Brown and W. D. M. Rae, NuShell@MSU, MSU-NSCL report, 2007 (unpublished).
[5] B. A. Brown and W. D. Rae, http://www.nscl.msu.edu/~brown/resources/resources.html (2008).
[6] R. A. Radhi, N. T. Khalaf, and A. A. Najim, Nucl. Phys. A **724**, 333 (2003).
[7] R. A. Radhi, A. K. Hamoudi, and K. S. Jassim, Indian J. Phys. **81**, 683 (2007).
[8] G. Bertsch, J. Borysowicz, H. McManus, and W. G. Love, Nucl. Phys. A **284**, 399 (1977).
[9] B. A. Brown, W. A. Richter, R. E. Julies, and B. H. Wildenthal, Ann. Phys. **182**, 191 (1988).
[10] A. Yokoyama, J. Phys.: Conf. Ser. **20**, 143 (2005).
[11] B. H. Wildenthal, Prog. Part. Nucl. Phys. **11**, 5 (1984).
[12] E. K. Warburton and B. A. Brown, Phys. Rev. C **46**, 923 (1992).
[13] E. K. Warburton, J. A. Becker, and B. A. Brown, Phys. Rev. C **41**, 1147 (1990).
[14] Y. Utsuno, T. Otsuka, T. Mizusaki, and M. Honma, Phys. Rev. C **60**, 054315 (1999).
[15] S. Nummela, P. Baumann, E. Caurier, P. Dessagne, A. Jokinen, A. Knipper, G. Le Scornet, C. Miehé, F. Nowacki, M. Oinonen, Z. Radivojevic, M. Ramdhane, G. Walter, and J. Äystö, Phys. Rev. C **63**, 044316 (2001).
[16] B. A. Brown and W. A. Richter, Phys. Rev. C **74**, 034315 (2006).
[17] W. A. Richter and B. A. Brown, Phys. Rev. C **80**, 034301 (2009).
[18] K. S. Jassim, Phys. Scr. **86**, 035202 (2012).

[19] J. R. Marinelli and J. R. Moreira, Phys. Rev. C **45**, 1556 (1992).
[20] B. A. Brown and B. H. Wildenthal, Annu. Rev. Nucl. Part. Sci. **38**, 29 (1988).
[21] M. Honma, T. Otsuka, B. A. Brown, and T. Mizusaki, Phys. Rev. C **69**, 034335 (2004).
[22] R. A. Radhi and A. Bouchebak, Nucl. Phys. A **716**, 87 (2003).
[23] P. J. Brussaard and W. M. Glaudemans, *Shell-Model Application in Nuclear Spectroscopy* (North-Holland, Amsterdam, 1977).
[24] T. W. Donnelly and I. Sick, Rev. Mod. Phys. **56**, 461 (1984).
[25] H. Nakada, Phys. Rev. C **68**, 014316 (2003).
[26] B. A. Brown, B. H. Wildenthal, C. F. Williamson, F. N. Rad, S. Kowalski, H. Crannell, and J. T. O'Brien, Phys. Rev. C **32**, 1127 (1985).
[27] R. B. Firestone, Nucl. Data Sheets **108**, 1 (2007).
[28] R. B. Firestone, Nucl. Data Sheets **110**, 1691 (2009).
[29] R. P. Singhal, A. Johnston, W. A. Gillespie, and E. W. Lees, Nucl. Phys. A **279**, 29 (1977).
[30] M. Shamsuzzoha Basunia, Nucl. Data Sheets **112**, 1875 (2011).
[31] B. A. Brown, W. Chung, and B. H. Wildenthal, Phys. Rev. C **22**, 774 (1980).
[32] P. P. Singhal, A. Watt, and R. R. Whitehead, J. Phys. G **8**, 1059 (1982).
[33] F. E. Cecil, R. F. Fahlsing, N. Jarmie, R. A. Hardekopf, and R. Martinez, Phys. Rev. C **27**, 6 (1983).
[34] L. Tassie, Aust. J. Phys. **9**, 407 (1956).
[35] R. A. Radhi, Nucl. Phys. A **707**, 56 (2002).
[36] H. Baghaei, A. Cichocki, J. B. Flanz, M. Frodyma, B. Frois, Y. Han, R. S. Hicks, J. Martino, R. A. Miskimen, C. N. Papanicolas, G. A. Peterson, S. Platchkov, S. Raman, S. H. Rokni, and T. Suzuki, Phys. Rev. C **42**, 2358 (1990).